Weak Motifs, Strong Complex: KANK1 Uses Cooperative Multivalency with the Hub-Protein LC8 to Bridge Cytoskeletal Complexes.

Douglas R. Walker[1], Aidan Estelle[1], York-Christoph Ammon[2], Anna Akhmanova[2], Elisar J. Barbar[1]

[1]Department of Biochemistry & Biophysics, Oregon State University, Corvallis, OR, United States

[2]Cell Biology, Neurobiology and Biophysics, Department of Biology, Faculty of Science, Utrecht University, Padualaan 8, Utrecht 3584 CH, the Netherlands.

ABSTRACT

KANK1 is a cytoskeletal regulator localized to the cortex of the cell, where it binds to both focal adhesions, which regulate the actin cytoskeleton, and cortical microtubule stabilizing complexes. The protein LC8 is a small dimeric protein that acts as a dimerization hub for many clients through binding at a short linear motif. Many LC8 clients bind the protein multivalently, through repetition of the LC8-binding linear motif. While the exact function of each multivalent LC8 client is unique, these interactions are thought to play a structural role, rigidifying a disordered region of the client protein. Here, we present work that demonstrates that despite containing only weak LC8 binding motifs, KANK1 binds multivalently to LC8, driving LC8's localization to the cell cortex. Due to the weakness and non-canonical character of the LC8 binding sites on KANK1, experiments illustrated that prediction with our algorithm LC8Pred is insufficient to find all sites. AlphaFold was used to complement LC8Pred and locate the remaining binding sites. KANK1-LC8 binding is highly cooperative, with an overall binding affinity at least two orders of magnitude greater than the affinity of each individual LC8-binding motif. This cooperativity results in a complex that favors a homogenous, fully bound state. Multivalent AlphaFold predictions suggest assembly as a kinked-rod-like structure. We believe this cooperative complex serves a structural role, with the cooperativity building a rod, elongating a large disordered linker and enabling it to reach across the gap between the cell membrane and the ends of microtubules.

SIGNIFICANCE STATEMENT

In this work we report KANK1 as the most homogeneous binder of LC8 that has been characterized. We show that, unintuitively, the strong homogeneous complexation is driven by weak individual binding motifs. This paper significantly expands the field's understanding of the breadth of different motifs to which LC8 can bind, requiring the use of structure-based AlphaFold binding-site predictions in concert with motif-based predictors in order to find all LC8 binding sites. These predictions suggest that KANK1 hosts more LC8 binding sites than any other LC8 partner that has been studied. Finally, the function of LC8/KANK1 complexation has been elusive, but structural predictions suggest that LC8 rigidifies and elongates the linker region of KANK1 to allow it to reach microtubule tips.

INTRODUCTION

LC8 is a small protein which self-assembles into a 20 kDa homodimer which acts as a binding hub via interaction with clients at a short linear motif (SLiM) found in intrinsically disordered regions (IDR/Ps)(1, 2). Hub proteins like LC8 interact with many binding partners, and are important regulators due to their position as central points of networks of protein-protein interactions(3, 4). The LC8-binding motif is characterized by a threonine-glutamine-threonine (TQT) amino acid triad which anchors clients within the binding site (Fig. 1a,b)(1, 5). LC8 has two rotationally symmetric binding grooves which enable accommodation of two client strands(6). In most situations, LC8 binds two copies of the same protein and induces or strengthens dimerization of the client (Fig. 1a)(2, 7–9).

Due to the simplicity of SLiMs, they are ideally suited to facilitate multivalent complexation: One protein can easily present several SLiMs along its sequence(10, 11). Such multivalent complexes frequently play essential roles in larger macromolecular assemblies where LC8-IDP duplexes act as scaffolds(10). LC8 partners are involved in a host of cellular functions: at the nuclear pore(12, 13), regulating transcription(14–16), at neuronal synapses(17), regulating the cytoskeleton during cell division(5), and more(18–20). Multivalent LC8 assemblies form beads-on-a-string "polybivalent" complexes, in which two strands of client IDP string through LC8 "beads"(10, 14), forming assemblies with varying rigidity. Owing to complex binding thermodynamics along with structural and stoichiometric heterogeneity, these complexes are challenging to study(14, 21). Investigation of multivalent LC8 complexes by ultracentrifugation or electron microscopy often indicates a high degree of structural heterogeneity. Although experimentally complicated, heterogeneity likely plays a functional role *in vivo*, as we proposed for transcription factor ASCIZ where heterogeneous binding enables sensing of LC8 concentration and regulation of its expression(14).

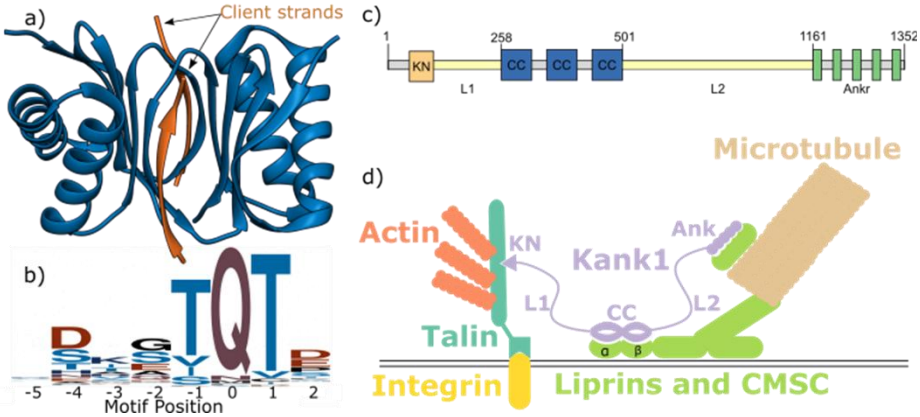

Figure 1: LC8 and KANK1 structure and function. (a) Ribbon diagram of LC8 (blue) with two client strands (orange) (PDB 2P2T). Clients take a beta-strand structure when bound to LC8. (b) Sequence logo of the LC8 motif, constructed from all known LC8-binding sequences in the LC8Hub database(1). (c) Diagram outlining KANK1 structure, including KN motif (orange), ankryin repeat domain (green), coiled-coils (blue) and linker sequences (yellow). (d) Schematic of KANK1 (purple) binding to FAs (left) and cortical microtubule stabilizing complexes (CMSCs) (right). KANK1 interacts with Talin1 (teal) to bind

FAs and is additionally recruited to CMSCs by liprins (light green) through interactions with the ankyrin and coiled-coil domains.

ASCIZ is one of the most studied LC8 multivalent binding partners(14–16, 21–27). Using ITC, AUC, and SEC-MALS, we showed that LC8/ASCIZ heterogeneity stems partially from a mix of high and low affinities in the binding motifs but also partially from a variety in inter-site linker lengths(27). In particular, the combination of a very short linker and a long linker makes for a prime example of heterogeneity in a three-site construct of dASCIZ. Conversely, a construct with mid-length linkers complexes with LC8 much more homogeneously. At least one long linker is present in ASCIZ across all species investigated, supporting the hypothesis that the long linker is important for functional heterogeneous binding.

We have shown that LC8 is present throughout the cytoplasm and the cell nucleus in interphase HeLa cells(1), however, it also is significantly concentrated in puncta at the cell cortex near focal adhesions (FAs). FAs contain more than 50 distinct types of proteins(28) that come together to form highly organized plaques at the plasma membrane(29). In addition, many other proteins associate near FAs such as cortical microtubule stabilizing complexes (CMSCs)(30, 31). Where LC8 interacts with FAs, CMSCs, or other nearby proteins is not known. The large number of proteins localized at these regions where LC8 is concentrated emphasizes the importance of technology developed for predicting partners and sites of LC8 binding.

We have developed two complementary computational methods for predicting LC8 binding partners. LC8Pred(1) was trained with the amino acid propensity at each position of the SLiM from known LC8 binding sites. LC8Pred predicts at least 374 potential LC8 binding sites in the human proteome. Secondly, we recently developed a method for using AlphaFold predictions of LC8 with small peptides parsed from the protein of interest to predict LC8 binding(32). While LC8Pred has the advantage that it was designed specifically for LC8, AlphaFold can predict LC8 binders which do not resemble those already known. Thus, these two techniques are complementary in their ability to interrogate a given protein sequence and its potential for binding LC8.

One promising contender for LC8 interaction is KANK1. KN motif and ankyrin repeat protein 1 (KANK1) is a ~150 kDa member of the KANK protein family (KANK1-4)(33, 34), which share an N-terminal KN motif and C-terminal ankyrin repeat domain(33–35). KANK1 shares many characteristics with known multivalent LC8-binding proteins: Beyond the KN motif and ankyrin repeat domain, KANK1 consists of a mix of predicted disorder and coiled-coil structure, including several coiled-coils predicted from residues 258-501 and two long stretches of predicted disorder, L1 and L2, spanning residues 60-258, and 501-1161 (Fig. 1c). KANK1 is a tumor suppressor(33, 36), and frequently found downregulated in cancer tissues in the kidney(36), brain(37, 38), and lungs(39). The mechanism of tumor suppressor activity

is unclear, but it may be connected to the role that KANK1 plays in regulating the cytoskeleton at the cell cortex.

KANK1 is further a promising candidate because, uniquely, it interacts with complexes which regulate actin and microtubule cytoskeletons(31, 35). The KN motif binds tightly to Talin1(35, 40, 41), a key player in forming focal adhesions (FAs), which anchor actin stress fibers (Fig. 1e). Additionally, KANK1's coiled-coil domains bind Liprin-β1, part of CMSCs (31), which regulate microtubule growth and attachment to the plasma membrane (Fig. 1d). The ankyrin repeat domain recruits the kinesin-4 KIF21A to CMSCs(31, 34, 35, 40, 42–45), which acts as a cortical microtubule growth inhibitor(31). As a member of both microtubule- and actin-regulating complexes, KANK1 offers a route for crosstalk between the two systems.

Here, we demonstrate that KANK1 binds LC8 in its disordered L2 region. We show that in HeLa cells, KANK1 is one of the major factors in LC8 localization, and recruits LC8 to the edges of FAs. Despite containing only a single canonical LC8 motif, multiple weak binding sites facilitate KANK1 binding LC8 multivalently, resulting in a cooperativity-driven ladder-like complex. We identify these binding sites through combination of peptide binding, LC8Pred, and AlphaFold predictions. Uniquely among multivalent LC8 complexes, the LC8/KANK1 complex is structurally homogenous. We determine that short linkers in concert with the weak motifs preclude alternative assemblies, leaving only the rigid aligned structure as viable, a situation which drives homogeneous complexation. Finally, through structural prediction and contextual mechanisms, we infer that the interaction between LC8 and KANK1 elongates the L2 domain to span the gap to microtubules as they approach the cell membrane.

RESULTS

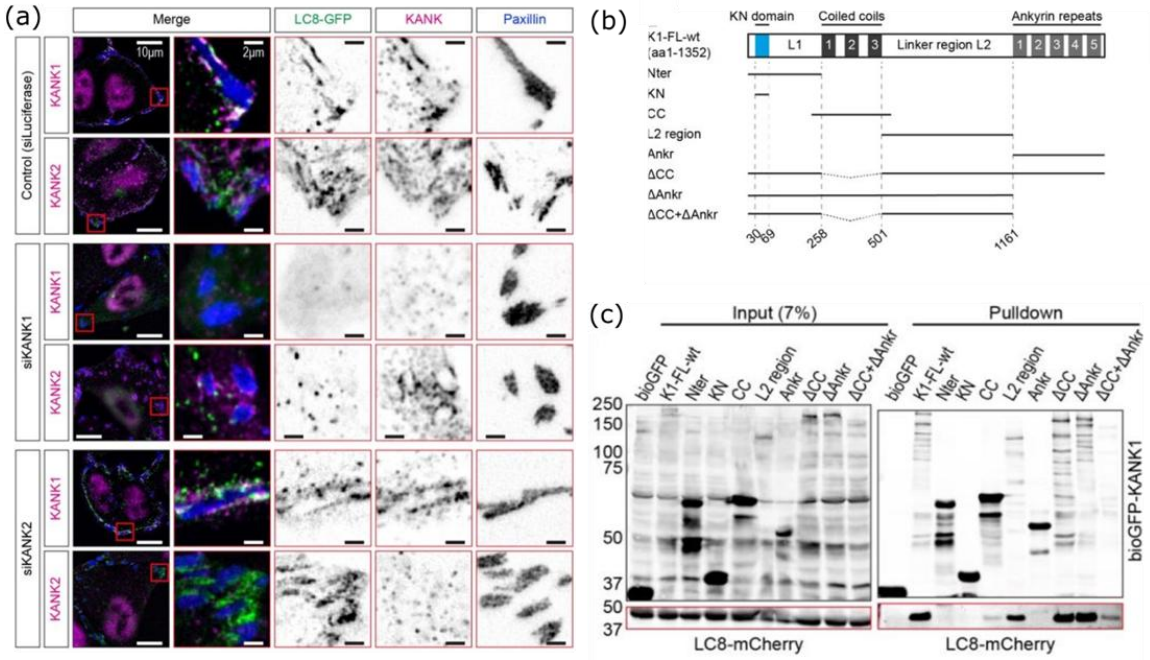

Figure 2: LC8 Colocalizes in KANK1 in HeLa cells. (a) Cells expressing LC8-GFP (green), stained for Paxillin (blue) and KANK1 or KANK2 (red). LC8 and KANK1 colocalize at the edges of focal adhesions. Cells are transfected with siRNA for luciferase (as a control), siKANK1 and siKANK2. Silencing of KANK1 abolishes LC8 colocalization. (b) Diagram of KANK1 structure, with bio-GFP tagged constructs designed for pulldowns shown. (c) Streptavidin pulldowns of LC8-mCherry with bioGFP-KANK1. Left is input of crude cell lysate being pulled down, while right are blotted for GFP (top) and mCherry (bottom).

KANK1 colocalizes with LC8 around focal adhesions

Pulldown mass spectrometry provided first evidence of interaction between KANK1 and LC8. KANK1 pulls down LC8 along with known KANK1-interacting proteins Talin1, Liprin-β1, and KIF21A(35, unpublished). To examine this interaction in cells, we stained for Paxillin (found in FAs), and KANK1 or KANK2 in HeLa cells stably expressing LC8 tagged with GFP (Figure 2a). LC8 signal strongly overlaps with KANK1 in patches at FA edges. LC8 and KANK2 do not co-localize, suggesting that the KANK1/LC8 interaction may be unique in the KANK family. Depletion of KANK1 via siRNA-mediated knockdowns eliminates localization of LC8 to FAs, confirming KANK1 as responsible for LC8's presence near FAs. Knockdown of KANK2 does not impact LC8 localization, confirming that KANK2 does not interact with LC8.

KANK1's intrinsically disordered L2 binds LC8

To determine the LC8-binding domain in KANK1, we performed streptavidin-based pulldown assays on LC8, using constructs of bioGFP-KANK1 as bait. This revealed that L2 (residues 501 - 1161) is where LC8 binds (Fig. 2b,c). L2 strongly pulls down LC8 on its own. Other constructs that bind LC8 all contain L2. Importantly, no other isolated domain pulls down LC8.

To further narrow the region, constructs containing fragments of L2 were used for pulldown assays (Figure 3a,b).

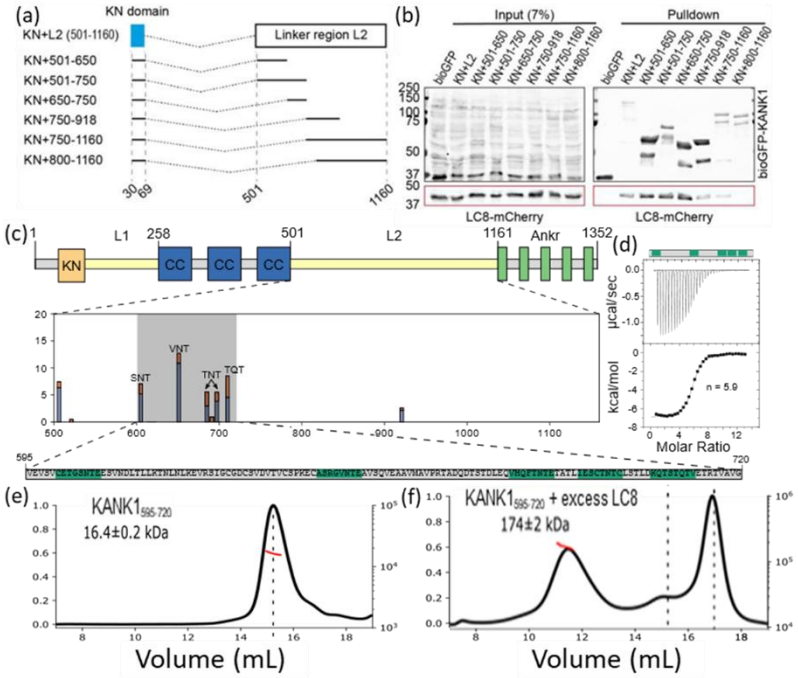

Figure 3: KANK1$_{595\text{-}720}$ binds LC8 multivalently. (a) KANK1 constructs with KN domain and L2 fragments to locate the LC8 binding region. (b) KN-L2 constructs pulldowns narrowing LC8 binding to KANK1$_{500\text{-}750}$ (c) KANK1 domain map showing folded (orange, blue, green) and disordered regions (yellow). Zoom shows LC8pred scores for the L2 region (500-1160). High density of low LC8Pred scores in KANK1$_{595\text{-}720}$ prompted biophysical characterization of this region. (d) Isotherm titration of LC8 with full KANK1$_{595\text{-}720}$. (e) SEC-MALS for free KANK1$_{595\text{-}720}$ and (f) with excess LC8 to study the ratio of the fully bound complex.

Constructs KN+501-750, 501-650, and 650-750 strongly pull down LC8, while constructs 750-918 and 750-1160 show weak pulldown and 800-1160 does not pull down LC8. This implicates residues 501-750 as containing the main LC8 binding domain with strong binding in 501-650 and 650-750, and weak binding in 750-800. We utilized LC8Pred(1) to predict LC8 binding in L2 and found that there no predicted binding sites surpass thresholds we established when developing LC8Pred to reduce false positive predictions. However, within residues 600-720, five motifs were found with low prediction scores (Figure 3c). The strongest predicted site has a sequence of ASRGVNTE with N as anchor instead of Q at residue 651. The other four are much weaker: a SNT motif at position 605, a VNT motif at 651, two TNT motifs at 685 and 697, and a TQT motif at 710. Despite low scores, the density of predicted sites prompts investigation.

KANK1 binds LC8 multivalently

To investigate binding between KANK1 and LC8, we recombinantly expressed residues 595-720 of L2 which includes all predicted LC8-binding motifs and performed isothermal titration calorimetry (ITC) experiments titrating LC8 into $KANK1_{595-720}$ (Figure 3d). We measured a binding affinity of 1.3 μM, with enthalpy of -6.6 kcal/mol, consistent with expectations for a tight-binding LC8-client complex. Notably, the Origin(46) calculated stoichiometry is 5.9, a very high ratio of LC8:KANK binding. While *n* is not always a trustworthy parameter in complex cases due to low precision in concentration measurements and assumptions in the independent-sites model(47), this high value of *n* can be taken as an indicator that KANK1 binds LC8 at multiple motifs. Since none of the predicted motifs exceed the established threshold of LC8Pred, yet LC8 binds $KANK1_{595-720}$ at several locations, this suggests that multivalency plays an important role in achieving the strong binding observed by ITC.

To provide further confirmation of binding stoichiometry we performed size exclusion chromatography-multiangle light scattering (SEC-MALS) experiments on $KANK_{595-720}$. First, examining the protein in isolation, we see a single dominant peak, suggesting a homogenous sample (Fig. 3e). The MALS mass of the peak is 16.4 kDa, matching the expected 16.4 kDa monomer mass of the construct. To examine the LC8/$KANK_{595-720}$ complex, we mixed $KANK_{595-720}$ with excess LC8 and SEC purified the complex. A dominant new peak for the complex is evident (Fig. 3f) and MALS mass measurements reports a complex mass of 174 kDa, which matches closely to the mass expected of a 14:2 LC8:$KANK_{595-720}$ complex (181 kDa). The mass along this peak is not uniform due in part to some dissociation of the complex on the SEC column, apparent in the presence of peaks corresponding to LC8 dimer and to monomer $KANK_{595-720}$. Nevertheless, the observed complex mass corroborates the high stoichiometry seen in ITC and suggests a 14:2 complex, where 7 LC8 dimers bridge two strands of $KANK1_{595-720}$.

KANK1-LC8 binding is highly cooperative

To investigate details of LC8-client binding and the affinity of the five predicted LC8-binding motifs in isolation, we synthesized peptides of each motif and measured binding to LC8 by ITC. None of the motif peptides bound to LC8 at an affinity measurable by ITC. The isotherm for peptide 1 shows no evidence of binding while isotherms for peptides 2 through 5 show only very weak binding, with isotherms 3 and 5 most closely approaching an acceptable binding curve (Fig. 4a). All isotherms were collected at an LC8 concentration of 60 μM, indicating that the affinity between LC8 and peptides is likely well above 60 μM in all cases. These results justify the low LC8Pred motif predictions in which none of these sites are expected to bind LC8. The contrast in the binding affinities of LC8 with KANK1 peptides or with KANK1$_{595\text{-}720}$ suggests that LC8-KANK1 complex formation is strongly driven by cooperativity between the multiple LC8 motifs within KANK1.

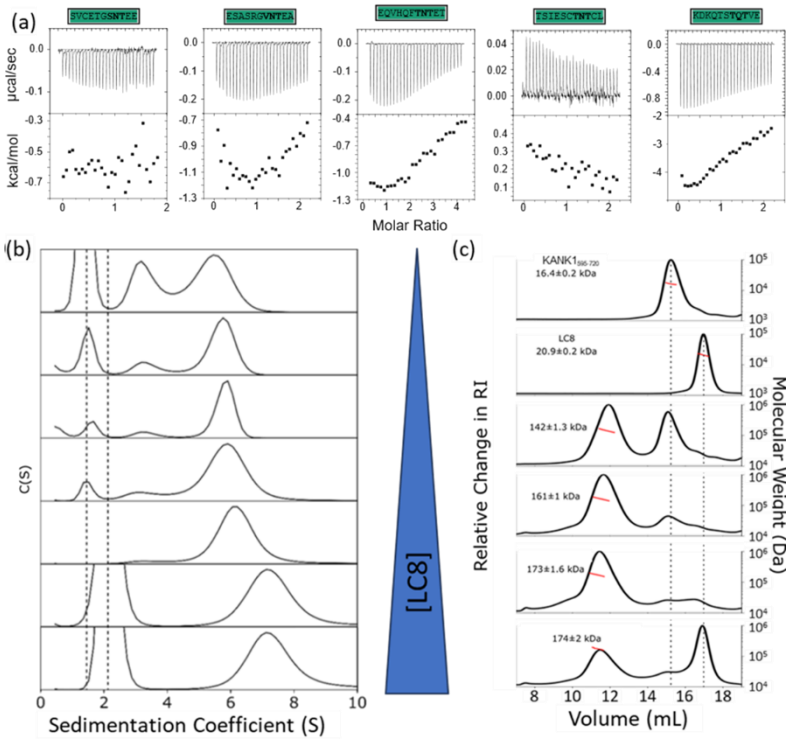

Figure 4: KANK1-LC8 binding is strongly cooperative. (a) ITC between LC8 and KANK1 peptides. (b) Titrations of KANK1$_{595\text{-}720}$ and LC8 by SV-AUC. y-axes normalized to tallest bound-state (>2.5 s) peak. (c) MALS of KANK1$_{595\text{-}720}$, LC8, and titration. RI normalized to highest intensity. Measured mass is in red with average mass listed. In (b,c) LC8 concentration increases in the lower plots. Dotted lines mark the positions of each protein alone.

A titration of LC8 into KANK1$_{595\text{-}720}$ by sedimentation velocity analytical ultracentrifugation (SV-AUC) confirms the strong binding cooperativity (Fig. 4b). At low LC8:KANK1$_{595\text{-}720}$ ratios, three AUC peaks are evident, one corresponding to free KANK1$_{595\text{-}720}$, one corresponding to an intermediate state at ~3 svedbergs (S), and one corresponding to a large complex at ~5.5 S. As the titration progresses, the minor intermediate species and the KANK$_{595\text{-}720}$ peaks both disappear. Specifically, a shift away from excess KANK$_{595\text{-}720}$ and towards a new peak for excess LC8 occurs at higher titration points, suggesting a saturated complex. At these same higher titration points, the bound state peak shifts from 6 S to 7 S. This could be due to a new distinct bound structure at these higher titrations. However, recalling that equilibrium exchange between partially and fully occupied states will impact the simple model used to analyze our SV

experiments, it is more likely that the shift seen in the latter titration points is due to a reduction in the exchange between partially and fully bound states and an equilibrium shift toward the fully bound state.

Finally, a SEC-MALS titration also corroborates strong binding cooperativity (Figure 4c). Low ratios of LC8 and KANK1$_{595-720}$ result in chromatograms exhibiting high mass complexes even when a large peak corresponding to excess KANK1$_{595-720}$ is still evident. Even before a peak for excess LC8 is observed, the complex reaches its maximum mass corresponding to a 14:2 complex. Dynamic exchange is once again apparent in this titration through the raised baseline between complex peaks and free protein peaks and by the range of masses measured by MALS for each peak. However, even in the diluting conditions of an SEC column and a starting concentration of 1 µM complex, this dynamic exchange is minimal, consistent with the high cooperativity and the strength of binding in the fully bound complex.

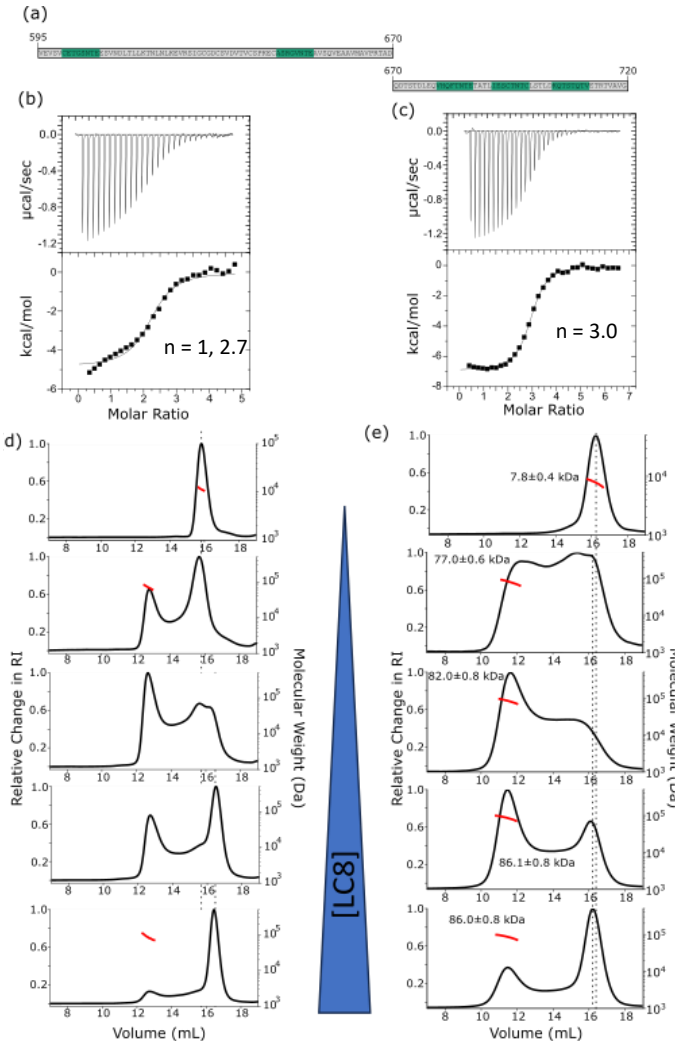

Fig 5: Kank1$_{595-670}$ and Kank1$_{670-720}$ both bind LC8 multivalently. (a) Short KANK1 constructs for locating binding sites. (b,c) ITC titrations of LC8 into Kank1$_{595-670}$ (b) and Kank1$_{670-720}$ (c). Fits are shown for a one-set-of-sites model. (d,e) MALS titration of 50 uM Kank1$_{595-670}$ (d) and Kank1$_{670-720}$ with LC8 (e). Top panel shows MALS trace of Kank1 construct alone. RI values are normalized to the highest intensity in the window shown. Red lines indicate measured masses for bound state peaks, with the average reported mass listed in each panel. Dotted lines indicate the expected elution times of apo Kank1 and LC8. Saturated complex masses correspond to 2:6 and 2:7 stoichiometries, respectively.

Shorter KANK1 constructs propose locations of the additional LC8 binding sites

To identify the location of the LC8 binding sites that were missed by LC8Pred, we made two additional constructs which divide KANK1$_{595-720}$ in two: KANK1$_{595-670}$, and KANK1$_{670-720}$ (Figure 5a). ITC of KANK1$_{595-670}$ (Figure 5b) exhibits a less cooperative isotherm than KANK1$_{595-720}$ with two transitions evident at *n* of 1 and 2.7 corresponding to one site which binds

somewhat independently and two which bind cooperatively while, the ITC of KANK1$_{670\text{-}720}$ (Figure 5c) shows a strong cooperative transition similar to KANK1$_{595\text{-}720}$ with n=3. However, SEC-MALS titration of KANK1$_{595\text{-}670}$ with LC8 immediately forms a peak with mass corresponding to a mixture of 2:4 and 2:6 (KANK:LC8, Figure 5d). As the titration progresses, the complex doesn't grow after the 2:6 ratio, indicating that KANK1$_{595\text{-}670}$ hosts 3 LC8 binding sites. KANK1$_{670\text{-}720}$ immediately exhibits a complex ratio of 2:6 (Figure 5e), but shows a mixture of 2:6 and 2:8 binding later in the titration. However, the 2:8 species never dominates even at large excesses of LC8, suggesting the presence of 4 binding site, with one weak enough that it dissociates on the column. In fact, the titrations of both smaller KANK1 constructs exhibit exchange, seen as tailing in the complex peak, on the SEC column, more than with KANK1$_{595\text{-}720}$, indicative

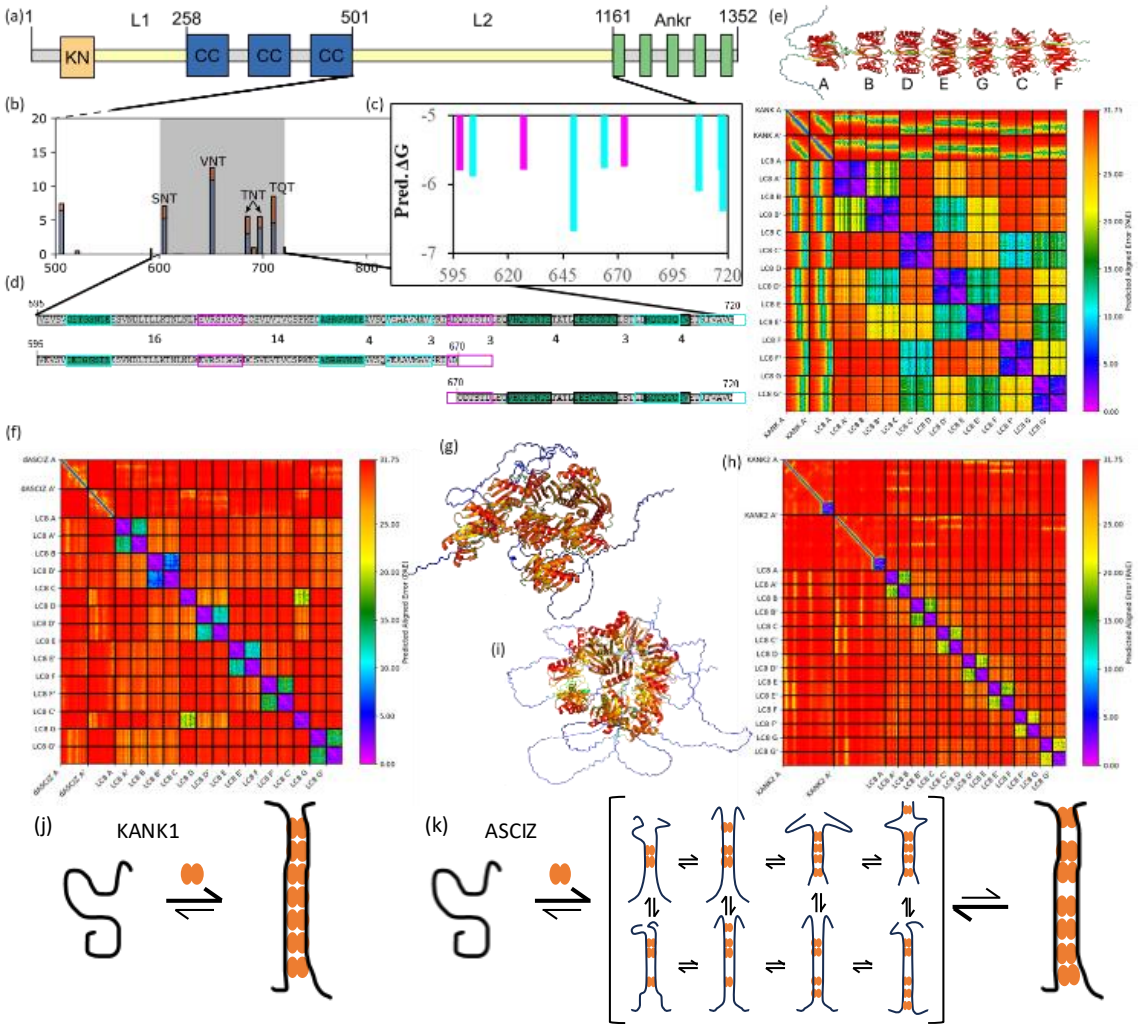

of weaker complexes. ITC of these constructs also report weaker binding than seen for the larger construct.

Figure 6: AlphaFold finds remaining LC8 binding sites. (a) Domain structure of Kank1 showing folded domains (orange, blue, green) and regions of disorder (yellow). (b) LC8pred scores for 500-800 are shown. (c) AlphaFold predictions for 595-720, the region spanned by experimental constructs, find the missing binding sites (colored boxes). Cyan results are from the exclusive threshold and magenta from the inclusive.

(d) Construct sequences with predicted sites boxed by prediction method: LC8Pred, black; AF exclusive, cyan; AF inclusive, magenta. (e) AlphaFold prediction of KANK1$_{595\text{-}720}$ with 7 LC8 dimers and the associated heatmap of pae values. Sequence LC8s are lettered according to their position in the heatmap. Heatmap colors indicate highest confidence in violet and lowest confidence in red. KANK residues bound to LC8s are much more confident than the surrounding sequence. (f) Heatmap of paes for AlphaFold prediction of dASCIZ$_{LBD}$ with 7 LC8 dimers and (g) the associated structure. (h) Heatmap of paes for AlphaFold prediction of KANK2-L2 with 7 LC8 dimers and (i) the associated structure. (j) Cooperative multivalency in KANK1$_{595\text{-}670}$ leads to homogeneous binding with LC8. (k) ASCIZ binds to LC8 in a heterogeneous ensemble in dynamic equilibrium.

AlphaFold predictions explain complex binding stoichiometries

While LC8Pred finds five potential LC8 binding sites in KANK1$_{595\text{-}720}$, our experiments show that this fragment binds to seven LC8 dimers meaning that LC8Pred misses two binding sites. We used AlphaFold according to our recently developed method(32) to complement our LC8Pred predictions (Figure 6a,b). We extracted the scores associated with AlphaFold structure predictions of LC8 with potential binding sites to predict whether the investigated sequence does indeed bind LC8. We parsed KANK1-L2 into 16 amino acid long peptides with 8 amino acids overlap between successive sections. AlphaFold predictions of LC8 dimers with each of the parsed peptides resulted in the predictions seen in Figure 6c,d. When developing this method, we established two different sets of thresholds to evaluate LC8 binding in different circumstances: The exclusive threshold has a lower false positive rate and is therefore more useful for screening new LC8-binding proteins, whereas the inclusive threshold has a lower false negative rate and is therefore better for detecting weak or uncommon binding sites in proteins already known to bind LC8, but not where LC8 binds.

The exclusive threshold finds five binding sites between residues 595 and 722, however, two of these predicted sites are new: a VMA motif anchored at 663 and a VGE motif anchored at 720 and thus partially cut off in KANK1$_{595\text{-}720}$ and KANK1$_{670\text{-}720}$. Interestingly, the AlphaFold prediction does not identify the TQT motif, but instead predicts a TST anchored motif two residues N-terminal of the TQT motif. It is noteworthy that the TQT motif is not evolutionarily conserved while the TST motif is conserved across animalia KANK1 sequences as either TST or TNT(48), giving more credence to the AlphaFold TST predicted site. The inclusive threshold finds two additional binding motifs: an IGC motif anchored at 629 and a TST motif anchored at 674. It is exciting that AlphaFold predicts five noncanonical LC8 binding sites, opening the door to further elucidation of the intricacies of LC8 binding.

While experiments indicate that there are seven binding motifs in KANK1$_{595\text{-}720}$, combining LC8Pred and AlphaFold predictions yields nine predicted LC8 binding sites. However, ITC analysis of the peptide SVCETGSNTEE, made to investigate the motif anchored at 605, exhibited no transition. Given that it is distal from the other LC8 binding sites, it is reasonable to conclude that this predicted site does not bind in the context of this construct. However, it may still bind in the full protein. Secondly, the predicted

VGE site anchored at 720 is not fully contained within the construct KANK1$_{595-720}$ and those missing residues are necessary for binding. Therefore, with added information that is not available to either prediction algorithm, of the nine predicted sites, two likely do not bind, matching our experimental observations. The density of the remaining seven sites, and the shortness of the linkers between them, explains the high cooperativity between the LC8 binding sites along the chain despite their individually weak affinities. In the shorter constructs, KANK1$_{595-670}$ binds to three LC8 dimers, consistent with the AlphaFold predictions of the IGC, VNT, and VMA anchored binding sites. KANK1$_{670-720}$ exhibits a less straightforward stoichiometry with a mixture of 1:3 and 1:4 binding. However, as shown in Figure 6d, the motif anchored at 674 is not fully present in this construct: it is missing two N-terminal residues. The lack of these two residues would result in weaker or transient binding of LC8 to this motif which is consistent with our experimental observations.

Proximal multivalent weak binding results in a rigid rod-like complex

We performed AlphaFold titrations on the LC8 binding regions of both KANK1 and dASCIZ, and of the L2 region of KANK2 for comparison (supporting information). Because dASCIZ binds heterogeneously, we were not expecting AlphaFold to produce a high-quality structure with seven LC8 dimers and two LC8 binding sites. We were, however, hopeful that the homogeneous nature of LC8/KANK1 binding would allow for confident structures of this complex. To our satisfaction, the KANK1 complex yielded a highly confident rod-like structure consisting of seven LC8 "beads" packed tightly on two parallel KANK1 "strings" (Figure 6e) whereas the dASCIZ prediction shows binding at known binding sites, albeit with low confidence, but produced a chaotic structure with little resemblance to what one might visualize in an LC8 partner complexation (Figure 6f,g). The KANK2-L2 predictions with seven LC8 dimers exhibit no interaction between KANK2 and LC8 dimers, instead preferring to optimally pack the LC8 dimers as if in a crystalline lattice and wrap this up in the KANK2 strands (Figure 6h,i). This difference is consistent with KANK2 not binding LC8 as we show in Figure 2a.

Despite our expectations, it is still curious that AlphaFold would perform so differently for these complexes. ITC fits give very similar binding affinities for each complex (1.3 μM for KANK1 and 1.4 μM for ASCIZ(14)) and the binding stoichiometries are identical. Despite these similarities, the pattern of predictions made by AlphaFold mirrors experimental results for these complexes: in both the AlphaFold and the experimental results, the KANK1 construct binds highly cooperatively resulting in a single stable species as observed by AUC (Figure 4). Conversely, the functional heterogeneity of the LC8/dASCIZ complex observed by AUC manifests in many different bound states all present simultaneously which is reflected in the low confidence of AlphaFold's prediction despite the strong binding affinity of the interaction. The differences between KANK2 and dASCIZ predictions illustrate that predictions of a heterogeneous binder will have low confidence but retain binding at the known binding sites and produce

a chaotic structure whereas a nonbinder will have low confidence and portray inconsistent binding sites or no binding, favoring instead a structure which optimizes packing of LC8 dimers.

Overall, the AlphaFold results of $KANK1_{595-720}$ binding to LC8 are consistent with experimental results. The maximal size of the complex as measured by SV-AUC matches that seen for the larger, minority complex that appears only when a large excess of LC8 is added to dASCIZ(14), which was presumed to correspond to the ladder-like structure of dASCIZ saturated by LC8. Additionally, the high degree of cooperativity, in concert with the stoichiometry obtained by MALS, suggests such an elongated beads-on-a-string-like structure.

Given that $KANK1_{595-720}$ and $dASCIZ_{LBD}$ are both about 120 residues in length, titrations were also run on 120 residue long sub-constructs of $KANK1_{800-1161}$ and of KANK2-L2 (supporting information) to confirm that differences in AlphaFold prediction behavior were not due to construct length exceeding some ideal length for observing the types of behaviors seen in Figure 6e,g. The results of the titrations with these sub-constructs are consistent with the 300-residue long $KANK2_{LBD}$ and do not show cooperativity or even suggestion of binding.

DISCUSSION

Lessons learned about multivalent binding

The stoichiometry of 7:1 LC8:$KANK1_{595-720}$ is reminiscent of ASCIZ/LC8 binding. However, their multivalent behaviors are very different, and this presents an opportunity to discuss the reasons for the presence and absence of cooperativity. Because of the nature of LC8 binding in dimerizing clients, one might expect all LC8 binding interactions with multivalent partners to exhibit cooperativity due to the increased effective concentration of the individual strands after the first LC8 “bridge” is formed. However, that is not what is observed for ASCIZ. In contrast, the individual weak binding sites in KANK1 result in cooperative, strong, homogeneous binding, while more stable sites in ASCIZ bind non-cooperatively and heterogeneously. Our previous work(27) suggested that both binding motif sequence and inter-motif linker length contribute to the behavior of a multivalent partner binding to LC8. This current work highlights the importance of homogeneity both in binding affinities and in linker lengths in promoting homogeneity of complex assembly. We hypothesize that the weakness of each individual binding site precludes the possibility of alternative complexes assembling due to overall low stability in all but the fully occupied, in-register complex. Further, the linker lengths in KANK1 (3-4 amino acids) are optimized for cooperativity, consistent with our conclusions in previous work(27). This implies that mismatched linker lengths and a spread in affinities in ASCIZ enable the formation of complexes, other than the fully occupied, in-register complex, which must disassemble before they can reassemble into the lowest energy state, which again is consistent with our previous work and can explain the heterogeneity and lack of cooperativity in LC8/ASCIZ binding. This is not the first system for which this sort of phenomenon has been observed:

Recent study of the rates of self-assembly of collagen triple helices found that the rate limiting step in the hours-to-months long process of folding a triple helix is actually unfolding of off-target triple helices(49). The parallel between LC8 multivalency and collagen triple helical assembly points to important considerations and a careful balance when considering complexes whose assembly is driven by multivalency. It highlights some methods biology uses to solve problems that humans classically do not, but maybe we should sometimes consider options that are not the strongest, most homogeneous, or most optimized. For instance, folding that is too strong may stabilize competing structures; optimized affinities may result in off-target binding.

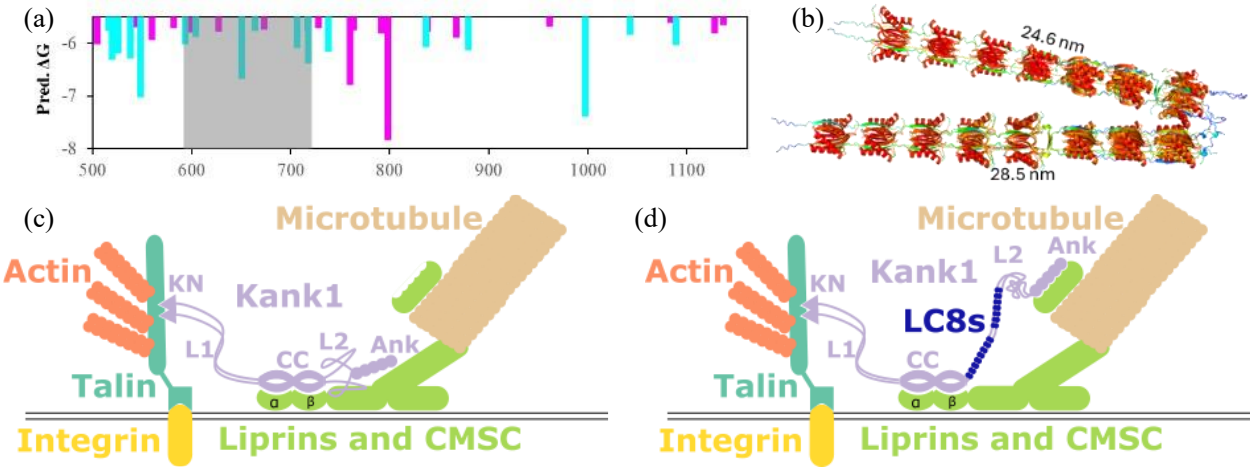

Figure 7: LC8 binding to KANK1 rigidifies L2 enabling reach between liprins and KIF2A. (a) AlphaFold predictions of LC8 binding across the full length of L2. Cyan and magenta correspond to predictions by the exclusive and inclusive thresholds respectively. (b) Aligned structures of predictions of $KANK1_{595\text{-}720}$, $KANK1_{500\text{-}615}$, and $KANK1_{541\text{-}670}$ with 7, 8, and 8 LC8 dimers, respectively, showing the potential of 15 simultaneous LC8 binding events with a bend at the nuclear export domain. (c,d) Models of accessible states of KANK1 interactions without and with LC8 binding. End-to-end distance for a random coil amounts to 9 nm on average, whereas interaction with LC8 rigidifies L2, allowing it to span the distance to KIF21A at the end of a microtubule.

Implications and hypotheses of the purpose of LC8/KANK1 interaction

In addition to the region of L2 implicated by LC8Pred, the entire length of L2 was predicted for LC8 binding (Figure 7a). Beyond residue 800 predicted motifs are sparse and weakly predicted, which is consistent with pull-down assays which show no LC8 binding in that region (Figure 3b). However, residues 500-600 display many predicted binding sites with weak affinities, but short linker lengths, as in $KANK1_{595\text{-}720}$. To investigate the possibility that LC8 rigidifies even more of KANK1-L2 than we studied experimentally, we ran AlphaFold titrations of $KANK1_{500\text{-}615}$ and $KANK1_{541\text{-}670}$. $KANK1_{500\text{-}615}$ titrations indicate an optimal stoichiometry of 1:8 KANK:LC8 which includes an LC8 bound to the most N-terminally LC8Pred predicted motif. We argued that this site does not bind in the context of $KANK1_{595\text{-}720}$ but may bind in the context of the full L2. $KANK1_{541\text{-}670}$ also binds eight LC8 optimally, but shows a 16-residue gap between adjacent binding regions which corresponds to the location of the nuclear export

domain. Structural alignment of KANK1$_{500-615}$, KANK1$_{541-650}$, and KANK1$_{595-720}$ each saturated with LC8, suggests flexible rigidification and elongation of the 250 residues of L2 (Figure 7b).

It is interesting to note that an estimate of the resulting length of this rigidified section of the protein is in excess of 50 nm. This matches the distance between integrins at the membrane surface and the tips of microtubules which grow toward CMSCs near FAs(50–52). Contrastingly, the average end-to-end distance between the N- and C- termini of L2 without LC8 bound would be about 9 nm (Figure 7e), as modeled by a simple random walk calculation: the length of a segment multiplied by the square root of the number of segments. This leads us to hypothesize that the purpose of LC8 binding to KANK1 in such a strongly cooperative manner as we have characterized is to elongate L2. Depending on the order of binding, this could enable it to set or just simply span the 50 nm gap between liprins, where the CC domain binds, and the tip of microtubules, where the Ank domain binds to KIF21A. It is of further interest to note that although KANK1 and KANK2 have similar affinity to KIF21A(43–45), and are both expressed in HeLa cells, KANK1 is much more dominant in controlling KIF21A localization and microtubule organization than is KANK2(31).

It is clear is that KANK1 is a first-of-its-kind LC8 interactor. It potentially binds 15 LC8 dimers, putting it in competition with human ASCIZ which binds 11-16 LC8 dimers for the LC8 partner with the highest known occupancy. No other known LC8 partner exhibits the extreme cooperativity of LC8 binding as does KANK1. No other known LC8 binder is quite as extreme in the use of such weak individual binding sites to assemble such a strong multivalent complex. Characterization of KANK1 binding to LC8 expands out understanding of the modes of LC8 client binding, the importance of weak binding interactions, and of consistent short linkers between adjacent motifs in promoting cooperativity. In addition, this system offers alternative perspectives on drug design, bioengineering, and even structural engineering, where optimizing for binding affinity, homogeneity, or strength may not be the best metrics on which to focus.

MATERIALS AND METHODS

Cell culture and DNA/siRNA transfections

HeLa (Kyoto) cells stably expressing LC8-GFP were a kind gift from I. Poser and A. Hyman (Max Planck Institute of Molecular Cell Biology and Genetics, Dresden, Germany)(53). HeLa cells were cultured in DMEM medium. HEK293T cells were cultured in DMEM:F10 medium (1:1, v/v). All media were supplemented with 10 % (v/v) fetal calf serum and with Penicillin/Streptomycin (100 units/mL penicillin and 100 µg/mL streptomycin). All cells were grown at 37 °C in humidified incubators at 5% CO2 atmosphere. The cells were routinely checked for mycoplasma contamination using the Mycoalert assay (Lonza, LT07-518).

Transfection of siRNA into HeLa cells and of DNA into HEK293T cells was performed as previously described(31). In brief, HeLa cells were transfected with siRNAs using HiPerFect (Qiagen). The siRNA-

transfected cells were analyzed 48 – 72 hours after transfection. The cells were analyzed 24 hours after DNA transfection. HEK293T cells were transfected with DNA using polyethyleneimine (PEI). The cells were harvested for pulldown assays around 24 hours after transfection.

DNA constructs and siRNAs

The BioGFP-tagged KANK1 and KANK2 fusion constructs were made using PCR-based amplification of different KANK1 or KANK2 fragments. These fragments were cloned into pBioGFP-C1 vector using Gibson Assembly mix (New England Biolabs) as described previously(35). The LC8-mCherry fusion construct was made by PCR-based amplification of LC8 and cloning it into the pmCherry-N1 vector.

The same siRNAs against KANK1 and KANK2 were used as described previously(35) to deplete HeLa LC8-GFP cells of KANK1 and KANK2: control siRNA (siLuciferase) GTGCGTTGCTAGTACCAAC; siKANK1 CAGAGAAGGACATGCGGAT; siKANK2 ATGTCAACGTGCAAGATGA.

Streptavidin-based pulldown assays

Streptavidin-based pulldown assays of biotinylated KANK constructs expressed using BioGFP-tagged-KANK constructs in HEK293T cells were performed as previously described(31). In brief, HEK293T cells were seeded in 10 cm plastic culture dishes to ~80 % confluence, the cells were allowed to attach overnight. The following day, the cells were transfected with the BioGFP-tagged KANK constructs together with biotin-ligase BirA (5µg DNA per construct) using PEI. In parallel, 1 – 2 10 cm plastic culture dishes were transfected with the prey protein only (LC8-mCherry, or HA-KANK1-FL, 10µg DNA) using PEI. The DNA/PEI suspensions were added to the cells dropwise. Thereafter, the cells were incubated for 24 hours at 37 °C in 5 % CO2 atmosphere in humidified incubators. After incubation, the cells were harvested on ice using ice-cold PBS and a spatula to scrape them from the dishes. The harvested cells were pelleted and subsequently lysed using a non-ionic detergent-based lysis buffer (50 mM HEPES pH 7.4, 150 mM NaCl, 1 mM EDTA, protease inhibitor cocktail (Roche), 1 % Triton-X100) for 10 minutes on ice. Afterwards, the suspension was centrifuged at 13,200 rpm at 4 °C for 15 minutes. In the meantime, the magnetic streptavidin beads (ThermoFisher, 11206D) were blocked in lysis buffer supplemented with 5% chicken egg white (Sigma) for 30 minutes at RT. Thereafter, the lysate of the prey protein was equally distributed among the biotinylated GFP-tagged KANK constructs. Thereafter, the lysate mixes were incubated with the streptavidin beads for 2 hours at 4 °C, except for 7 % of each lysate mix which was kept as "input" control. DTT-containing SDS-PAGE protein sample buffer was added to the input control. After incubation of the lysates with the streptavidin beads, the beads were washed 5 times using the lysis buffer and a magnetic "DynaMag" rack (ThermoFisher, 12321D). Thereafter, DTT-containing SDS-PAGE protein sample buffer was added to the beads.

The following SDS-PAGE and Western blot analysis were performed according to standard procedures. Commercially available antibodies against GFP (Abcam, ab6556), mCherry (clone 1C51, Abcam,

ab125096) and HA (clone 16B12, BioLegend/Covance, MMS-101P) were used. For the detection, near infrared fluorescence technology was used (Li-Cor Biosciences, Odyssey system), using infrared dye conjugated goat antibodies against mouse and rabbit (Li-Cor Biosciences).

siRNA-mediated knockdown of KANK1 and KANK2 in HeLa LC8-GFP cells

HeLa LC8-GFP cells were seeded were seeded in 6-well culture plates and transfected using 20nM per siRNA per well using HiPerFect (Qiagen) and adding the siRNA/transfection reagent mix to the cell suspension. The cells were allowed to attach and to incubate in the siRNA/transfection reagent-containing medium overnight. The following day, the cells were washed 2-times with PBS and incubated for another 24 hours. The following day (~48 hours after siRNA transfection), the cells were trypsinized and seeded on 12mm glass coverslips (10,000 – 15,000 cells per coverslip) and allowed to attach overnight. The following day (~72 hours after siRNA transfection), the cells were washed with PBS and fixed for immunofluorescence staining.

Antibodies and Immunofluorescence staining

Cell fixation and staining were performed as previously described(31). In brief, the cells were fixed with ice-cold methanol for 7 minutes at -20 ºC. After one-time washing with PBS, the cells were permeabilized for 4 minutes at room temperature (RT) using permeabilization buffer (0.2 % TritonX-100 (Sigma) in PBS). Thereafter, the cells were blocked in blocking buffer (0.05 % Tween-20 (Sigma) and 2 % BSA (Carl Roth) in PBS) for 1 hour at RT. After blocking, the cells were incubated with primary antibodies diluted in blocking buffer for 1 hour at RT. After incubation, the cells were washed 5 times for 2 minutes with wash buffer (0.05 % Tween-20 in PBS); followed by 1 hour incubation with the fluorescently labeled secondary antibodies diluted in blocking buffer. The cells were washed 5 times for 2 minutes with wash buffer and afterwards, dehydrated using first 70 % and then 100 % ethanol. Finally, the coverslips were mounted on glass slides using Vectashield mounting medium (Vector laboratories, H-1000).

Commercially available antibodies against KANK1 (Atlas antibodies, HPA005539), KANK2 (Atlas antibodies, HPA015643), and paxillin (clone 165, BD Biosciences, 610620) were used. Alexa-405, Alexa-488 and Alexa-594 conjugated goat antibodies against rabbit and mouse IgG were purchased from Invitrogen.

Microscopy and image analysis

Images of fixed cells were collected with a Nikon Eclipse Ni upright wide field fluorescence microscope and a Nikon DS-Qi2 CMOS camera (Nikon), using Plan Apo Lambda 100x N.A. 1.45 oil objective (Nikon) and Nikon NIS (Br) software (Nikon). Nikon Intensilight C-HGFI was used as a light source. For imaging of blue, green and red fluorescence the filter sets ET-BFP2 (49021), ET-GFP (49002), and ET-mCherry (49008) (all Chroma) were used respectively.

For presentation, images were adjusted for brightness and contrast using ImageJ 1.50b (NIH).

Protein Expression and Purification

For all biophysical assays, LC8 and KANK1$_{595-720}$ were expressed recombinantly in E. coli. Proteins were cloned into the pET24d expression vector, with an N-terminal 6xHis and TEV-cleavable site and expressed in either Rosetta (LC8) or C41 (KANK1$_{595-720}$) E. coli cells, both of which are derived from BL21 DE3 cells. Cells were grown in ZYM5052 auto-induction media at 37 C for 24 hours. LC8 and KANK1$_{595-720}$ were both purified by affinity chromatography with TALON cobalt resin, as previously described(14). KANK1$_{595-720}$ expresses into inclusion bodies and was therefore purified using buffers containing 8 M urea as previously described(14). Following affinity purification, KANK1$_{595-720}$ was dialyzed out of urea, and both KANK1$_{595-720}$ and LC8 were further purified by size exclusion chromatography (SEC) using a Superdex S75 hi-load column (GE Healthcare). SEC was performed in a buffer of 25 mM Tris, pH 7.5, 150 mM NaCl, 5 mM β-mercaptoethanol, and 1 mM NaN_3. Purified proteins were stored in SEC buffer either used within a week or flash frozen to -80 C for storage.

Isothermal titration calorimetry

We performed isothermal titration calorimetry at 25 °C with a VP-ITC microcalorimeter (Microcal) in SEC buffer. For KANK1$_{595-720}$, LC8 was titrated into a cell sample of KANK1$_{595-720}$, with a syringe and cell concentration of 400 and 4 μM respectively. Each injection had an 8 μL volume, and a total of 36 injections were performed. For KANK1 peptides, which were synthesized in-house using solid-phase synthesis and purified by HPLC, peptide was dissolved into SEC buffer at 500 μM and was titrated into a cell sample of LC8 at 60 μM. A total of 28 injections of peptide into LC8 were performed, at injection volumes of 10 μL. Peaks were integrated and fit to the n-independent sites model in Origin 7.0.

Analytical Ultracentrifugation

We performed sedimentation velocity analytical ultracentrifugation (SV-AUC) on a Beckman Coulter Optima XL-A analytical ultracentrifuge, equipped with optics for absorbance measurements. We mixed purified LC8 and KANK1$_{595-720}$ at a series of increasing concentrations, with a fixed KANK1$_{595-720}$ concentration of 7.2 μM, and at increasing LC8 concentration varied from 9 μM (1.25:1) to 144 μM (20:1). The 1.25, 2.5, and 3.75:1 complexes were measured by absorbance at 280 nm, 5 and 10:1 used absorbance at 292 nm, and the 15 and 20:1 complexes used 298 nm. All experiments were performed in SEC buffer, dialyzed the night before SV-AUC was performed, to ensure minimal β-mercaptoethanol degradation. We loaded the complexes into 12 mm path-length 2-channel cells, and centrifuged the samples at 42,000 rpm and 20 C. We acquired 300 scans at the relevant wavelength, with no delay between scans. Absorbance profiles were fit to a c(S) distribution in SEDFIT, with a calculated buffer density of 1.0009 g/ml, calculated using Sednterp.

Size exclusion chromatography – multiangle light scattering

For size exclusion chromatography paired with multiangle light scattering (SEC-MALS), experiments were performed on a 10/300 Superdex 200 analytical SEC column (GE Healthcare) attached to an AKTA-FPLC (GE Healthcare) and routed through a DAWN multiangle light scattering and Optilab refractive index system (Wyatt Technology). We equilibrated the system to SEC buffer, then injected 100 µL of sample onto the column. For $KANK1_{595-720}$ we injected a sample of 30 µM $KANK1_{595-720}$, and for the titrations we injected 2 µM $KANK1_{595-720}$ with increasing concentrations of LC8. Molar masses were estimated in the ASTRA software package, using a Zimm scattering model.

AlphaFold LC8 motif predictions

LC8 binding motifs predictions were achieved as previously described(32). Briefly, the sequences of the proteins to be investigated were parsed int 16 amino acid long segments with 8 residues of overlap between successive parsed peptides. The resultingly parsed peptides were then used in AlphaFold predictions in which an LC8 dimer was predicted with one and with two copies of the parsed peptide to simulate the half-bound and the fully bound state. In-built AlphaFold metrics were then extracted and compared to thresholds previously derived for both exclusive (low false positive, high false negative) and inclusive (low false negative, high false positive) cutoffs.

AlphaFold protein titrations

Two copies of sequences of full proteins or of sub-constructs were predicted with increasing numbers of LC8 dimers up to and beyond the number of binding sites that were identified by the motif prediction analysis. PAE heatmaps of the highest ranked prediction were analyzed and compared throughout the titration to confirm AlphaFold confidence and saturation point. The constructs experimentally investigated herein, $KANK1_{595-720}$, $KANK1_{595-670}$, and $KANK1_{670-720}$, were titrated with LC8 in addition to the $dASCIZ_{LBD}$ and $KANK2_{L2}$ regions as controls. Due to the quality performance of AlphaFold with protein segments of ~120 residues in length we also ran all sequences that were longer than 300 residues in parsed sections of 100-130 residues in length. PAE heatmaps of the best predictions for each titration point of all titrations run are included in the Supporting Information.

Acknowledgements

Y.-C. A. was supported by the Marie Skłodowska-Curie Actions Innovative Training Network (ITN) 675407 PolarNet.

References

1. N. Jespersen, *et al.*, Systematic identification of recognition motifs for the hub protein LC8. *Life Sci. Alliance* **2**, e201900366 (2019).

2. E. Barbar, Dynein Light Chain LC8 Is a Dimerization Hub Essential in Diverse Protein Networks. *Biochemistry* **47**, 503–508 (2008).

3. K. Komurov, M. White, Revealing static and dynamic modular architecture of the eukaryotic protein interaction network. *Mol. Syst. Biol.* **3**, 110 (2007).

4. N. Jespersen, E. Barbar, Emerging Features of Linear Motif-Binding Hub Proteins. *Trends Biochem. Sci.* **45**, 375–384 (2020).

5. S. Clark, A. Nyarko, F. Löhr, P. A. Karplus, E. Barbar, The Anchored Flexibility Model in LC8 Motif Recognition: Insights from the Chica Complex. *Biochemistry* **55**, 199–209 (2016).

6. G. Benison, P. A. Karplus, E. Barbar, Structure and dynamics of LC8 complexes with KXTQT-motif peptides: swallow and dynein intermediate chain compete for a common site. *J. Mol. Biol.* **371**, 457–468 (2007).

7. A. I. Kidane, *et al.*, Structural Features of LC8-Induced Self Association of Swallow†. *Biochemistry* **52**, 10.1021/bi400642u (2013).

8. N. E. Jespersen, *et al.*, The LC8-RavP ensemble Structure Evinces A Role for LC8 in Regulating Lyssavirus Polymerase Functionality. *J. Mol. Biol.* **431**, 4959–4977 (2019).

9. E. L. Eastwood, *et al.*, Dimerisation of the PICTS complex via LC8/Cut-up drives co-transcriptional transposon silencing in Drosophila. *eLife* **10**, e65557 (2021).

10. S. A. Clark, N. Jespersen, C. Woodward, E. Barbar, Multivalent IDP assemblies: Unique properties of LC8-associated, IDP duplex scaffolds. *FEBS Lett.* **589**, 2543–2551 (2015).

11. H. Y. J. Fung, M. Birol, E. Rhoades, IDPs in macromolecular complexes: the roles of multivalent interactions in diverse assemblies. *Curr. Opin. Struct. Biol.* **49**, 36–43 (2018).

12. A. Nyarko, Y. Song, J. Nováček, L. Žídek, E. Barbar, Multiple Recognition Motifs in Nucleoporin Nup159 Provide a Stable and Rigid Nup159-Dyn2 Assembly. *J. Biol. Chem.* **288**, 2614–2622 (2013).

13. M. Gaik, *et al.*, Structural basis for assembly and function of the Nup82 complex in the nuclear pore scaffold. *J. Cell Biol.* **208**, 283–297 (2015).

14. S. Clark, *et al.*, Multivalency regulates activity in an intrinsically disordered transcription factor. *eLife* **7**, e36258 (2018).

15. P. Rapali, *et al.*, LC8 dynein light chain (DYNLL1) binds to the C-terminal domain of ATM-interacting protein (ATMIN/ASCIZ) and regulates its subcellular localization. *Biochem. Biophys. Res. Commun.* **414**, 493–498 (2011).

16. O. Zaytseva, *et al.*, The Novel Zinc Finger Protein dASCIZ Regulates Mitosis in Drosophila via an Essential Role in Dynein Light-Chain Expression. *Genetics* **196**, 443–453 (2014).

17. A. Fejtova, *et al.*, Dynein light chain regulates axonal trafficking and synaptic levels of Bassoon. *J. Cell Biol.* **185**, 341–355 (2009).

18. A. Gupta, D. R. Diener, P. Sivadas, J. L. Rosenbaum, P. Yang, The versatile molecular complex component LC8 promotes several distinct steps of flagellar assembly. *J. Cell Biol.* **198**, 115–126 (2012).

19. L. K. Slevin, E. M. Romes, M. G. Dandulakis, K. C. Slep, The mechanism of dynein light chain LC8-mediated oligomerization of the Ana2 centriole duplication factor. *J. Biol. Chem.* **289**, 20727–20739 (2014).

20. K. L. West, *et al.*, LC8/DYNLL1 is a 53BP1 effector and regulates checkpoint activation. *Nucleic Acids Res.* **47**, 6236–6249 (2019).

21. B. Mostofian, *et al.*, Continuum dynamics and statistical correction of compositional heterogeneity in multivalent IDP oligomers resolved by single-particle EM. *J. Mol. Biol.* **434**, 167520 (2022).

22. S. Jurado, *et al.*, Dual Functions of ASCIZ in the DNA Base Damage Response and Pulmonary Organogenesis. *PLoS Genet.* **6**, e1001170 (2010).

23. S. Jurado, *et al.*, ATM Substrate Chk2-interacting Zn2+ Finger (ASCIZ) Is a Bi-functional Transcriptional Activator and Feedback Sensor in the Regulation of Dynein Light Chain (DYNLL1) Expression. *J. Biol. Chem.* **287**, 3156–3164 (2012).

24. S. Jurado, *et al.*, The Zinc-finger protein ASCIZ regulates B cell development via DYNLL1 and Bim. *J. Exp. Med.* **209**, 1629–1639 (2012).

25. A. King, *et al.*, Dynll1 is essential for development and promotes endochondral bone formation by regulating intraflagellar dynein function in primary cilia. *Hum. Mol. Genet.* **28**, 2573–2588 (2019).

26. P. N. Reardon, *et al.*, The dynein light chain 8 (LC8) binds predominantly “in-register” to a multivalent intrinsically disordered partner. *J. Biol. Chem.* **295**, 4912–4922 (2020).

27. D. R. Walker, *et al.*, Linker Length Drives Heterogeneity of Multivalent Complexes of Hub Protein LC8 and Transcription Factor ASCIZ. *Biomolecules* **13**, 404 (2023).

28. R. Zaidel-Bar, S. Itzkovitz, A. Ma’ayan, R. Iyengar, B. Geiger, Functional atlas of the integrin adhesome. *Nat. Cell Biol.* **9**, 858–867 (2007).

29. H. Wolfenson, Y. I. Henis, B. Geiger, A. D. Bershadsky, The heel and toe of the cell’s foot: A multifaceted approach for understanding the structure and dynamics of focal adhesions. *Cell Motil.* **66**, 1017–1029 (2009).

30. G. Lansbergen, A. Akhmanova, Microtubule Plus End: A Hub of Cellular Activities. *Traffic* **7**, 499–507 (2006).

31. B. van der Vaart, *et al.*, CFEOM1-associated kinesin KIF21A is a cortical microtubule growth inhibitor. *Dev. Cell* **27**, 145–160 (2013).

32. D. R. Walker, G. Fujimura, J. M. Vanegas, E. J. Barbar, Successful prediction of LC8 binding to intrinsically disordered proteins sheds light on AlphaFold’s black box. *Front. Mol. Biosci.* **12**, 1531793 (2025).

33. N. Kakinuma, Y. Zhu, Y. Wang, B. C. Roy, R. Kiyama, Kank proteins: structure, functions and diseases. *Cell. Mol. Life Sci. CMLS* **66**, 2651–2659 (2009).

34. Y. Zhu, N. Kakinuma, Y. Wang, R. Kiyama, Kank proteins: A new family of ankyrin-repeat domain-containing proteins. *Biochim. Biophys. Acta BBA - Gen. Subj.* **1780**, 128–133 (2008).

35. B. P. Bouchet, *et al.*, Talin-KANK1 interaction controls the recruitment of cortical microtubule stabilizing complexes to focal adhesions. *eLife* **5**, e18124 (2016).

36. S. Sarkar, *et al.*, A novel ankyrin repeat-containing gene (Kank) located at 9p24 is a growth suppressor of renal cell carcinoma. *J. Biol. Chem.* **277**, 36585–36591 (2002).

37. Z. Cui, *et al.*, KANK1 inhibits cell growth by inducing apoptosis through regulating CXXC5 in human malignant peripheral nerve sheath tumors. *Sci. Rep.* **7**, 40325 (2017).

38. X. Guo, W. Fan, X. Bian, D. Ma, Upregulation of the Kank1 gene-induced brain glioma apoptosis and blockade of the cell cycle in G0/G1 phase. *Int. J. Oncol.* **44**, 797–804 (2014).

39. Y. Gu, M. Zhang, Upregulation of the Kank1 gene inhibits human lung cancer progression in vitro and in vivo. *Oncol. Rep.* **40**, 1243–1250 (2018).

40. Z. Sun, *et al.*, Kank2 activates talin, reduces force transduction across integrins and induces central adhesion formation. *Nat. Cell Biol.* **18**, 941–953 (2016).

41. M. Yu, *et al.*, Force-Dependent Regulation of Talin–KANK1 Complex at Focal Adhesions. *Nano Lett.* **19**, 5982–5990 (2019).

42. N. Kakinuma, R. Kiyama, A major mutation of KIF21A associated with congenital fibrosis of the extraocular muscles type 1 (CFEOM1) enhances translocation of Kank1 to the membrane. *Biochem. Biophys. Res. Commun.* **386**, 639–644 (2009).

43. Q. Guo, *et al.*, Structural basis for the recognition of kinesin family member 21A (KIF21A) by the ankyrin domains of KANK1 and KANK2 proteins. *J. Biol. Chem.* **293**, 557–566 (2018).

44. W. Pan, *et al.*, Structural insights into ankyrin repeat–mediated recognition of the kinesin motor protein KIF21A by KANK1, a scaffold protein in focal adhesion. *J. Biol. Chem.* **293**, 1944–1956 (2018).

45. Z. Weng, Y. Shang, D. Yao, J. Zhu, R. Zhang, Structural analyses of key features in the KANK1·KIF21A complex yield mechanistic insights into the cross-talk between microtubules and the cell cortex. *J. Biol. Chem.* **293**, 215–225 (2018).

46. MicroCal, Data Analysis in Origin. (1998).

47. A. B. Estelle, A. George, E. J. Barbar, D. M. Zuckerman, Quantifying cooperative multisite binding in the hub protein LC8 through Bayesian inference. *PLOS Comput. Biol.* **19**, e1011059 (2023).

48. M. R. Hensley, *et al.*, Evolutionary and developmental analysis reveals KANK genes were co-opted for vertebrate vascular development. *Sci. Rep.* **6**, 27816 (2016).

49. C. C. Cole, *et al.*, Heterotrimeric collagen helix with high specificity of assembly results in a rapid rate of folding. *Nat. Chem.* **16**, 1698–1704 (2024).

50. M. J. Paszek, *et al.*, Scanning angle interference microscopy reveals cell dynamics at the nanoscale. *Nat. Methods* **9**, 825–827 (2012).

51. P. Kanchanawong, *et al.*, Nanoscale architecture of integrin-based cell adhesions. *Nature* **468**, 580–584 (2010).

52. S. J. Stehbens, *et al.*, CLASPs link focal-adhesion-associated microtubule capture to localized exocytosis and adhesion site turnover. *Nat. Cell Biol.* **16**, 558–570 (2014).

53. I. Poser, *et al.*, BAC TransgeneOmics: a high-throughput method for exploration of protein function in mammals. *Nat. Methods* **5**, 409–415 (2008).